Nucleic Acids Research, 2025, **53**, gkaf141
https://doi.org/10.1093/nar/gkaf141
Chemical Biology and Nucleic Acid Chemistry

Fluorogenic oligonucleotide cleavage probes with a branched linker improve RNA detection

Bruktawit Maru[1], Ayodele Edinboro[1,2], Adam Katolik[2], Roberto El-Khoury[2], Kaleena Basran[2], Alexander S. Wahba[2,3], Masad J. Damha[2,4,*], Nathan W. Luedtke[1,2,4,*], Maureen McKeague[1,2,4,*]

[1]Department of Pharmacology and Therapeutics, McGill University, Montreal H3G 1Y6, Canada
[2]Department of Chemistry, McGill University, Montreal H3A 0B8, Canada
[3]McGill Chemistry Characterization (MC[2]), McGill University, Montreal H3A 0B8, Canada
[4]Centre de recherche en biologie structurale, McGill University, Montreal H3G 0B1, Canada

[*]To whom correspondence should be addressed. Emails: maureen.mckeague@mcgill.ca
Correspondence may also be addressed to Nathan W. Luedtke. Email: nathan.luedtke@mcgill.ca
Correspondence may also be addressed to Masad J. Damha. Email: masad.damha@mcgill.ca

Abstract

Fluorescent probe-based quantitative polymerase chain reaction (qPCR) is essential for DNA/RNA quantification widely used in research and clinical diagnostics. The performance of fluorogenic probes depends heavily on their design, particularly the identities of the fluorophore and quencher moieties, and the linkers used to attach them to oligonucleotides. Here we report a highly modular, three-way branched glycerol 'X' linker in fluorogenic TaqMan® type oligonucleotide probes for multiplexed, reverse transcription qPCR (RT-qPCR). The flexible 'X' linker served as an internal attachment point for various quenchers (BHQ1, BHQ2) in probes containing a variable fluorophore at the 5′ end (Flu, Hex, Cy5, Cy5.5). A four-color RT-qPCR 'tetraplex' assay was thereby developed for distinguishing between RNA genomes from SARS-CoV-2, influenza A, and influenza B viruses in a single reaction. The 'X' linker exhibited superior performance with single-molecule detection limits approaching four copies, compared to an internal arabinoside-based (ara) linker strategy, demonstrating the presence of competing processes during primer extension, one where Taq exonuclease activity cleaves the fluorogenic X probe leading to productive fluorescence, and the second where the ara probe is displaced from the PCR template without cleavage. Together these results demonstrate the importance of linker structure selection in oligonucleotides for developing highly effective fluorogenic probes for qPCR.

Graphical abstract

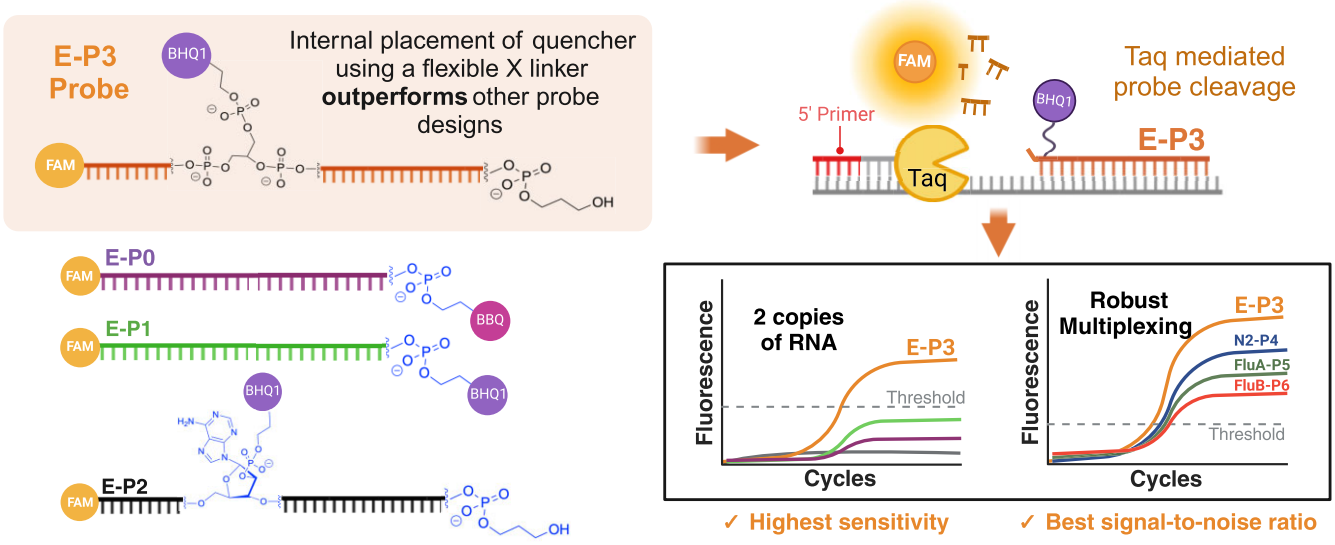

Received: October 15, 2024. **Revised:** January 25, 2025. **Editorial Decision:** February 10, 2025. **Accepted:** February 16, 2025

Introduction

Real-time quantitative polymerase chain reaction (qPCR) is the gold standard method for simultaneous amplification and quantitative detection of gene transcripts and genomes [1, 2]. The method is based on the principle of polymerase chain reaction (PCR), where DNA or complementary DNA (cDNA) templates are amplified through cycles of denaturation, annealing, and extension. Unlike traditional PCR, qPCR tracks the DNA amplification process via fluorescent dyes or probes in real-time, enabling precise quantification of target nucleic acids. The real-time detection of qPCR amplicons was first achieved using intercalating dyes such as ethidium bromide or SYBR Green that exhibit increased fluorescence intensities when bound to duplex DNA [3, 4]. Intercalator dye-based qPCR assays are relatively easy to design and cost effective to implement, but they are prone to false positives resulting from non-specific amplification, and they are incompatible with most multiplexing strategies [5]. In addition, intercalating agents can inhibit the PCR reaction itself, leading to diminished detection sensitivity [3]. These limitations motivated the development of new methods for specific and sensitive detection of qPCR amplicons [6, 7].

Using radioactive probes and gel electrophoresis, Holland *et al.* were the first to suggest that the 5′–3′ exonuclease activity of *Thermus aquaticus* (Taq) DNA polymerase could generate a specific, detectable signal during PCR amplification [8]. This concept was applied to the development of dual labeled fluorogenic qPCR probes containing a fluorophore covalently labeled on the 5′ end of the oligonucleotide, and a fluorescence quencher located at the 3′ end or an internal position of the oligonucleotide [9–11]. Hybridization of the probe to the PCR amplicon and primer extension coupled with the 5′–3′ exonuclease activity leads to increased fluorescence due to the cleavage of the fluorophore from the quencher. Hence, fluorescence increases can be directly proportional to the amount of amplicon being generated, allowing for accurate quantification of DNA and RNA copy numbers [10]. Multiple sets of fluorogenic dual labeled oligonucleotide hydrolysis probes and PCR primers, each with a different color and designed for a different nucleic acid sequence, can be used for high-throughput, multiplex assays [12, 13]. Together these features secured qPCR hydrolysis (or TaqMan®) probes as the gold-standard for detection of pathogenic organisms including viruses [1]. In practice, the proprietary technical details surrounding the development of such assays can lead to a broad range of copy number limits of detection, from 1 to 1000 genome copies [14]. As such, numerous studies have focused on optimization of the qPCR probes and primers for optimal sensitivity and specificity [6, 15, 16].

In addition to TaqMan probes, several strategies have been developed aimed to enhance the sensitivity, specificity, or versatility of qPCR probes (Supplementary Table S4). A common probe strategy is to use a molecular beacon that forms a stem-loop structure. In this structure, the end-labeled fluorophores and quenchers are in proximity but upon hybridization to the target sequence, the labels are spatially separated thereby producing a fluorescent signal [17–19]. While molecular beacons are specific and well-suited for multiplex assays, their dependence on precise stem-loop formation makes them less efficient than TaqMan probes [18, 19]. Another notable option includes the use of scorpion probes that combine primers and probes into a single molecule, enabling rapid signal generation and reducing false positives. However, their design complexity and limited compatibility with certain target sequences are major drawbacks [18, 20]. Modifications to probes, including the use of locked nucleic acids have also been employed to enhance hybridization stability and mismatch discrimination, although they require careful optimization to maintain efficiency [18,19,21]. Despite these diverse innovations, TaqMan probes remain the most widely used due to their simplicity, reliability, and established performance.

There are efforts to improve TaqMan probe performance, including the development of dual-quenched probes (e.g. ZEN and TAO) [22]. Such probes incorporate an internal quencher alongside a 3′-end quencher, offering enhanced fluorescence quenching and improved signal-to-noise. However, the proprietary chemistries used to prepare these probes can impede further probe innovations, and the lack of exact structural details of commercial probes can limit interpretations of reaction product analyses from qPCR reactions. These challenges highlight the need for advancement in TaqMan probe design, particularly in understanding how linker chemistry and internal quencher placement impact qPCR performance. The exact location of the conjugated quencher within a TaqMan probe is a crucial feature that dictates efficiency. Currently, probes with a quencher located at the 3′ end are widely used in qPCR [6, 23, 24]. However, internally placed quenchers have shown potential for improving quenching efficiency, thereby enhancing the signal-to-noise ratio and assay performance [6, 11, 22, 25]. Despite these advantages, the structural and functional relationships between the linker chemistry and internal placement of quencher and key qPCR parameters, such as sensitivity and efficiency, remain underexplored.

The widespread use of qPCR during the COVID-19 pandemic and its ongoing application in viral detection assays [24, 26–28] motivated our investigation of new quencher linker chemistries for internal placement to enhance qPCR sensitivity and multiplexing capabilities. Here we introduced various dark quenchers into probes using a glycerol-based branching linker ‘X’ which was designed to be a bulge rather than a nucleobase conjugate or a terminal label. This unique design enhances flexibility, reduces sequence constraints, and supports modular synthesis, thereby facilitating compatibility with diverse quenchers and enabling multiplexing applications. Alongside the glycerol-based linker, we tested a sugar-modified araA linker to compare the impact of linker site rigidity versus flexibility on probe performance. Our results demonstrate that during primer extension, a competition between probe cleavage (Fig 1, path A) and probe displacement (Fig 1, path B) is impacted by the structure of the linker between the quencher and internal position of the oligonucleotide. A comparison of the two types of internal quencher-linking strategies revealed that a simple, non-native backbone linkage comprising a glycerol unit enables outstanding cleavage efficiency. Using the glycerol linker ‘X’ in a SARS-CoV-2 E-gene probe and primer set developed by Corman *et al.* [24] for the diagnosis of COVID-19, we achieved near single-copy detection of the SARS-CoV-2 genome. The ‘X’ linker was furthermore utilized in the development of a four-color, multiplexed assay for distinguishing between SARS-CoV-2, influenza A, and influenza B viruses using quantitative reverse transcription PCR (RT-qPCR). Together, our studies on qPCR probes have yielded significant insights on how linker structure can impact probe cleavage and introduced novel probe

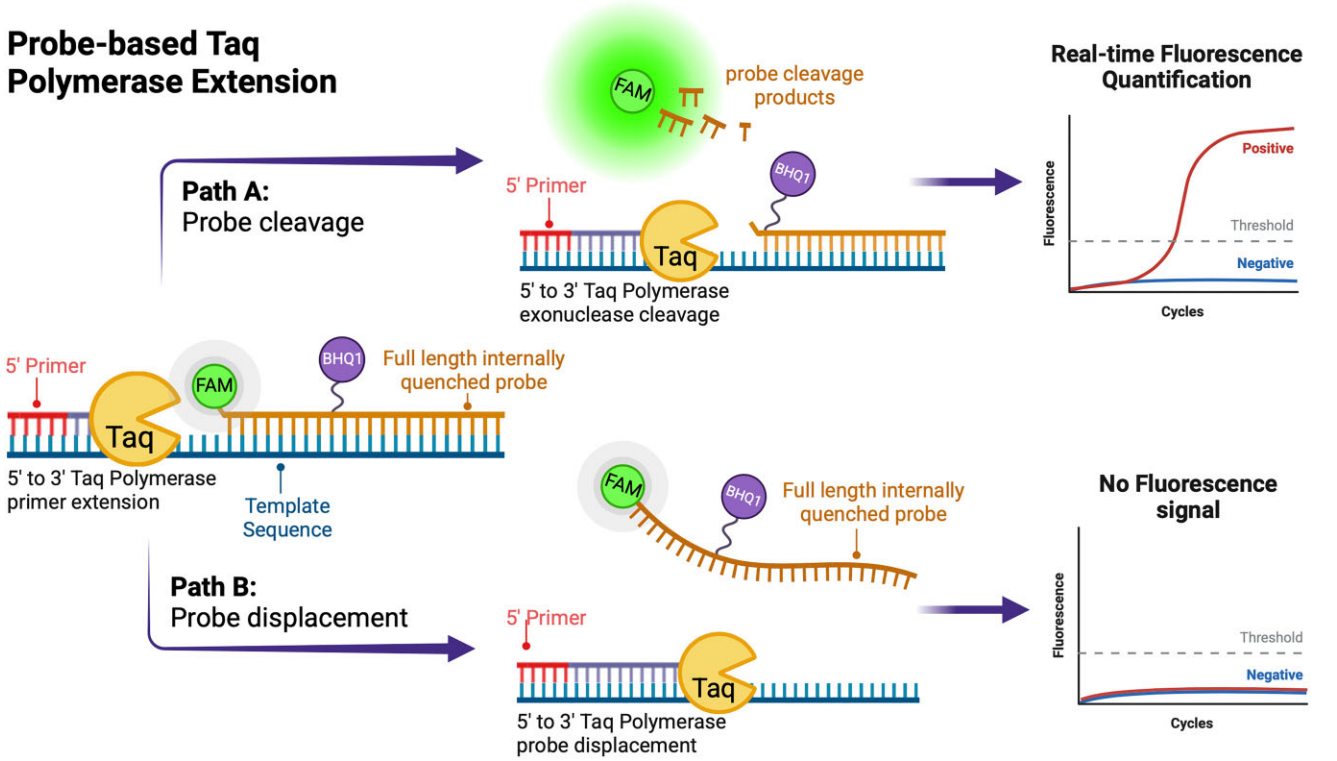

Figure 1. Competing pathways during Taq primer extension. Path A: Taq 5′–3′ exonuclease cleavage of the probe thereby separating the fluorophore and quencher and leading to higher measured fluorescence. Path B: Taq The probe is displaced from the PCR template giving little or no change in measured fluorescence. Figure created in BioRender. Maru, B. https://BioRender.com/e60f386.

chemistry that holds great promise for enhancing the reliability and efficiency of RT-qPCR for clinical diagnostics.

Materials and methods

Materials and reagents

We synthesized **E-P0**, **E-P2**, **E-P3**, **N2-P4**, **FluA-P5**, and **FluB-P6** probes as well as the E-gene primers E-F (E-gene forward primer) and E-R (E-gene reverse primer) and the N-gene primers N-F and N-R (Supplementary Tables S1 and S2). **E-P1** probe was purchased with high-performance liquid chromatography (HPLC) purification from BioCorp (Pierrefonds, QC, Canada) (Supplementary Table S2). The Influenza A forward and reverse primers (FluA-F and FluA-R) and the Influenza B forward and reverse primers (FluB-F and FluB-R) were ordered from ATCC® Genuine Nucleics (Manassas, VA, USA) (Supplementary Table S1). The one-step RT-qPCR Master Mix was made by McGill University according to published procedures [29] or purchased from Promega. All SARS-CoV-2 RNA was obtained from Twist Bioscience (South San Francisco, CA, USA). Influenza A RNA (10^5 copies) and Influenza B RNA (10^5 copies) were ordered from ATCC® Genuine Nucleics. The S1 Nuclease enzyme and S1 Nuclease buffer were obtained from Promega Corporation (Madison, WI, USA). Water Ultra-pure was purchased from Bio Basic Inc. (Markham, ON, Canada). The CFX96 Touch Real-Time PCR Detection System used for all RT-qPCR experiments was manufactured by Bio-Rad (Hercules, CA, USA). All RT-qPCR reactions were centrifuged in PlateFuge Microplate microcentrifuge from Montreal Biotech Inc. (Montreal, QC, Canada). Fluorescence polarization readings were taken using the BioTek Cytation 5 from Agilent (Santa Clara, CA, USA).

Solid phase synthesis of probes

In general, probes were synthesized on either an Applied Biosystems ABI 3400 or a Bioautomation MerMade 12 oligonucleotide synthesizer, using a scale of 1–3.3 μmol based on resin loading. Ancillary reagents were obtained from ChemGenes Corporation, including: (1) trichloroacetic acid/dichloromethane (TCA/DCM) for DMT removal; (2) 5-ethylthio-1H-tetrazole [0.25 M in acetonitrile (ACN)] as the activator; (3) 0.1 M I_2 solution in pyridine/H_2O/tetrahydrofuran (THF) for oxidation (0.02 M I_2 solution for coupling Cy3 and Cy5.5); (4) acetic anhydride/pyridine/THF and 16% N-methylimidazole in THF for capping. HPLC grade ACN was sourced from Fisher Scientific, and ACS grade DCM (for post-detritylation washes) was obtained from a BRAUN NM-SPS solvent drier. The synthesis utilized standard DNA phosphoramidites [dA (n-bz), dC (n-acetyl), dG (n-ibu), and dT], mild N-acetyl dG, or ultra mild phosphoramidites (dA ANP-6661, dC ANP-6662, and dG ANP-5668) from ChemGenes. 6-fluorescein amidite (FAM) (CLP-9777) was also purchased from ChemGenes, while 5′-hexachloro-fluorescein (1360547-55-2), Cyanine 3 (182873-76-3), Cyanine 5.5 (10-5916-90), BHQ1 (10-5931-90), and BHQ2 (10-5932-90) phosphoramidites were obtained from Glen Research. The arabinoadenosine-lev monomer was prepared as described previously [30]. The asymmetric branching phosphoramidite (CLP-7169) was sourced from ChemGenes. Solid supports were acquired from Glen Research, either BBQ-CPG 20-5934 or 3′ spacer CPG

(Glen Research G904440). To ensure anhydrous conditions, drying traps-XL (ChemGenes DMT-1972) were added to both ACN and the activator at least 2 h before synthesis.

Synthesis of **E-P0** was carried out using a MerMade 12 on a 3.3 μmol scale. BBQ-CPG (100 mg) was weighed into a manually cut syringe-style M15-1000 column (5.5 cm height) to fit the synthesizer chuck. Standard DNA amidites were dissolved in anhydrous ACN (<10 ppm) to a concentration of 100 mM. The synthesis cycle included: (i) three detritylation steps, (ii) two coupling steps, (iii) one capping step, and (iv) one oxidation step, with substantial washing and vacuum drying periods in between. Each detritylation reaction used 1500 μl of TCA and lasted 60 s. Coupling reactions lasted 120 s for dA, dC, and dT, and 180 s for dG, delivering 500 μl of phosphoramidite and 550 μl of activator. Capping reactions involved 850 μl of each reagent for 100 s, and oxidation steps delivered 10 000 μl of I_2 solution for 60 s. The 6-FAM phosphoramidite was coupled under the same conditions after completing the DNA portion of the synthesis. Probe **E-P1** was purchased from BioCorp (Pierrefonds, QC, Canada).

Synthesis of **E-P2** was performed on the ABI 3400 DNA synthesizer at a 1 μmol scale using the 3′-spacer C3 CPG. The first stage involved coupling the deoxyphosphoramidites and phosphoramidites araA and FAM. Phosphoramidites dA, dC, and dT were coupled for 200 s, while dG (N-ibu) was coupled for 300 s, and 6-FAM for 600 s. The araA phosphoramidite, a modified arabinose adenosine unit protected at the 2′ position with an orthogonally labile levulinic ester (LEV) group, was used at 0.1 M in anhydrous DCM:ACN (3:1) and coupled for 400 s. The second stage involved delevulyination of araA, using a freshly prepared 0.5 M hydrazine hydrate solution in pyridine/AcOH (3:2 v/v) flowed through the synthesis columns (20 s flow + 3.75 min hold, repeated four times). The solid support was then washed with ACN for 10 min. The final stage involved manually coupling the BHQ1 phosphoramidite to the free 2′-hydroxyl group. The synthesizer column containing the solid support was dried *in vacuo* for 15 min. BHQ1 amidite (20–25 mg) was dissolved in 0.1 ml of dry DCM/ACN (3:1), then mixed with 0.4 ml of dry 5-ethylthio-1H-tetrazole (0.25 M in ACN). This BHQ1 solution was passed through the synthesizer column, mixing back and forth over 2 h. The oxidation solution (0.1 M I_2/pyridine/H_2O/THF) was then passed similarly for 1 min after thoroughly rinsing the solid support with ACN. The synthesis of **E-P3** followed the same protocol as **E-P2**, but an asymmetric branch point phosphoramidite was used instead of araA.

FluA-P5 and **FluB-P6** were synthesized on a MerMade 12, with all phosphoramidites dissolved in anhydrous ACN at 100 mM. Detritylation reactions (two) were each delivered using 500 μl of TCA and reacting for 50 s. Coupling reactions lasted 800 s for dA, dC, and dT, and 1200 s for dG, delivering 250–300 μl of phosphoramidite and 300 μl of activator. Capping reactions delivered 250 μl of each reagent for 100 s, while oxidations used 700 μl of I_2 solution for 88 s. The first phase of synthesis coupled the DNA portion downstream of the branch point, using standard DNA phosphoramidites (for **N2-P4** and **FluA-P5**) or N-acetyl dG (for **FluB-P6**). The asymmetric branch point phosphoramidite was then coupled (800 s for N2-P8, two times 1200 s for **FluA-P5** and **FluB-P6**), with the DMTr group remaining intact. The levulinyl group was removed by applying a freshly prepared 0.5 M hydrazine hydrate solution in pyridine/AcOH (3:2 v/v) for 1200 s, delivered automatically to the column through a spare port. After extensive ACN washes, the column was dried under reduced pressure for over 30 min. The quencher (BHQ1 or BHQ2) phosphoramidite was coupled (1200 s for **N2-P4**, 1600 s for **FluA-P5**, and two times 800 s for **FluB-P6**), followed by the addition of the next DNA portion using ultra mild phosphoramidites. The use of standard DNA phosphoramidites in the first phase balances the need for complete deprotection and the stability of the cyanine dyes. Finally, the fluorescent dye was coupled (1600 s for **FluA-P5** and two times 800 s for **FluB-P6**). Probes **FluA-P5** and **FluB-P6** required an oxidizer change to a 0.02 M I_2 solution, necessitating four oxidation reactions to compensate for the lower concentration. A final detritylation step was performed to remove the MMTr group included in their respective synthons. After synthesis, the **FluA-P5** probe was treated with an anhydrous freshly made solution of diethylamine:ACN (1:9 v/v) for 1200 s to ensure removal of all cyanoethyl protecting groups, converting the phosphate triester internucleotide linkages to phosphate diesters, thereby stabilizing the molecule and preventing acrylonitrile adduct formation.

Deprotection of oligonucleotides

Prior to deprotection, all compounds were thoroughly washed with ACN and then dried under reduced pressure. The **E-P0** probe and the 3.3 μmol scale of the **E-P3** probe were transferred to a 15 ml sterile screw-cap tube, and 10 ml of 30% ammonium hydroxide was added. The samples were shaken for 48 h. Afterward, the product was briefly centrifuged, and the supernatant was distributed into two 10 ml sterile tubes, with 5 ml of supernatant in each. These tubes were opened and placed in a fume hood for at least 1 h. They were then closed and placed in a −20°C freezer for ∼15 min before being transferred to a rotary evaporator to remove the ammonium hydroxide under reduced pressure. The residue was dissolved in 1 ml of DEPC-treated, autoclaved MilliQ water, combined, and filtered into new sterile tubes. For compounds **E-P2**, **E-P3** (ABI 3400 synthesis), **FluA-P5**, and **FluB-P6**, the oligonucleotides were transferred to a 1.5 ml screw-cap sterile tube. In the case of compounds **E-P2** and **E-P3**, cleavage of the oligonucleotide from the CPG and removal of the nucleobase protecting groups were achieved by adding 1000 μl of aqueous ammonium hydroxide (30%) and methylamine (40%) (1:1) for 10 min at 65°C. For **FluA-P5** and **FluB-P6**, deprotection was performed by adding 1000 μl of aqueous ammonium hydroxide (30%) for 24 h at room temperature. After centrifugation, the solution was transferred to a clean tube, vented for 30 min, chilled in dry ice, and evaporated to dryness. The residue was then re-dissolved in 1 ml of DEPC-treated, autoclaved MilliQ water and filtered into a new sterile tube.

Purification of oligonucleotides

Crude oligonucleotides were purified by anion exchange HPLC on a Waters 1525 instrument using a column with Source 15Q resin (3 cm × 11.5 cm) at a flow rate of 10 ml/min and a column temperature of 60°C. Mobile phases included A (3:1 water: ACN with 13.5 mM sodium acetate) and B (3:1 water: ACN with 0.1 M lithium perchlorate and 13.5 mM sodium acetate). The gradients were as follows: 0%–75% B over 100 min for **E-P0**; 0%–100% B over 50 min for **E-P2**, and **E-P3**; 0%–100% B over 100 min for **N2-P4**; and 0%–75% B over 150 min for **FluA-P5** and **FluB-P6** probes, the latter of which required a second purification. **E-P2** underwent a sec-

ond purification by reverse phase HPLC on a Varian ProStar instrument using a C8-Aqua 5 μm column (10 mm × 150 mm) at a flow rate of 3.0 ml/min, employing a gradient of 5%–60% ACN over 30 min in 0.1 M triethylammonium acetate (pH 7.2). Samples were subsequently desalted on NAP-25 desalting columns according to the manufacturer's protocol. Masses were verified by high-resolution liquid chromatograph mass spectrometry (LC-MS) (Supplementary Table S3), described below. Concentrations were measured using a CARY 300 BIO UV-Vis spectrophotometer and adjusted to 100 μM stock solutions.

Oligonucleotide verification via LC-MS

Samples were analyzed by LC-MS using a Dionex Ultimate 3000 coupled to a Bruker Maxis Impact QTOF in negative electrospray ionization (ESI) mode. In a short method, samples were run through a Phenomenex Luna C18 (2)-HST column (2.5 μM, 120 Å, 2.1 × 50 mm) using a gradient of 98% mobile phase A (100 mM hexafluoro-2-propanol and 5 mM triethylamine in H_2O) and 2% mobile phase B (MeOH) to 40% mobile phase A and 60% mobile phase B in 8 min. In a long method, samples were run through a Phenomenex Luna C18 (2)-HST column (2.5 μM, 120 Å, 2.1 × 100 mm) using a gradient of 98% mobile phase A and 2% mobile phase B to 40% mobile phase A and 60% mobile phase B in 16 min. The data were processed and deconvoluted using the Bruker DataAnalysis software version 4.2.

RT-qPCR amplification of genes by different probe designs

For each probe, a 20× stock solution was prepared containing 4 μM of probe, 12 μM of forward primer, and 12 μM of reverse primer. Each 20× probe (1 μl) and primer mix was added to singleplex reactions containing 10 μl of in-house Master Mix and 5 μl of SARS-CoV-2 RNA, resulting in a final volume of 20 μl. A no-template control (NTC) was also included for each probe and primer mix, in which no SARS-CoV-2 RNA was added. The plate was centrifuged to pool the contents of each well. RT-qPCR was performed on the CFX96 Touch Real-Time PCR Detection System (Bio-Rad) using the following thermal cycling conditions: one cycle of reverse transcription at 53°C for 10 min, one cycle of polymerase activation at 95°C for 2 min, followed by a standard two-step cycling qPCR profile for dual-labeled hydrolysis probe detection consisting of 45 cycles of denaturation at 95°C for 15 s and annealing/extension at 60°C for 30 s. Finally, samples were cooled down with one cycle at 40°C for 30 s. For multiplex RT-qPCR, 20× probe and primer mixes targeting the E and N genes of SARS-CoV-2, as well as Influenza A and B, were combined in equal amounts of either 0.5 μl or 1 μl in each 20 μl RT-qPCR reaction.

Limit of detection using serial dilution of SARS-CoV-2 RNA

The copy number of SARS-CoV-2 RNA was unknown; therefore, using RNA with a known copy number (10^5 copies) from Twist Bioscience [Twist Synthetic SARS-CoV-2 RNA Control 1 (MT007544.1)], SARS-CoV-2 was approximated to be 10^6 copies using the method described below. Serial dilutions (~10^5, 10^4, 10^3, 10^2, and 10^1) of SARS-CoV-2 template RNA were prepared. For each gene, 1 μl of the corresponding 20× probe and primer mix was combined with 10 μl of McGill in-house Master Mix, 5 μl of each RNA dilution, and water to a final volume of 20 μl. Similarly, serial dilutions (10^4, 10^3, 10^2, 10^1, and 10^0) of Influenza A and Influenza B template RNAs were prepared, and 5 μl of RNA was combined with the corresponding 20× probe and primer mix, 10 μl of McGill in-house Master Mix, and water to a final volume of 20 μl. The same thermal cycling conditions described in the RT-qPCR protocol above were used.

Polyacrylamide gel electrophoresis assay

To confirm that each of the probes was being cleaved and amplifying the target, denaturing 10% polyacrylamide gels were prepared by first combining 15 ml of 40% acrylamide with 3 ml of 10× tris/borate/ethylenediaminetetraacetic acid (TBE) buffer. Urea (12.6 g) was dissolved in 11.2 ml of water and combined with TBE and acrylamide. Fifteen milligrams of ammonium persulfate (dissolved in 150 μl of water) and 30 μl of tetramethylethylenediamine (TEMED) were added to the gel mix, which was then immediately poured into a gel apparatus. While the gel polymerized, 5 μl of a 10× dilution of each thermal denaturation qPCR product was combined with 5 μl of formamide and incubated at 95°C for 5 min. After the gel polymerized, 10 μl of ultra-low range gene ruler ladder and the entire 10 μl of each sample were loaded into separate wells, and the gel was run at 120 V for 1 h. The unstained gel was imaged using a ChemiDoc MP Imaging System (Bio-Rad). Subsequently, the gel was stained with SYBR Gold for 30 min and then imaged again.

Thermal denaturation (T_m) assay

To observe the melting behavior of each probe, 200 nM of each probe was combined with 300 nM of the respective complementary sequence, 2 μl of EDTA (pH 8), and 1× qPCR Master Mix to a final reaction volume of 20 μl with Milli-Q water. The qPCR plate was then centrifuged in a microplate microcentrifuge (MBI) and run in the CFX96 Touch Real-Time PCR Detection System (Bio-Rad) using thermal cycling conditions starting at 25°C, followed by an increase to 95°C in 0.5°C increments every 10 s.

Fluorescence polarization assay

A 4× dilution of the samples from the thermal denaturation assay was made using Milli-Q water and equilibrated to 60°C. Fluorescence polarization measurements were taken using the BioTek Cytation 5 plate reader with a green fluorescence polarization filter (optical filter cube #8040561, Agilent) at 60°C. Parallel and perpendicular fluorescence were recorded using an excitation wavelength of 485/20 nm and an emission wavelength of 528/20 nm.

S1 nuclease assay

Each probe (1 μl of **E-P0**, **E-P1**, **E-P2**, and **E-P3**) was combined with 3 μl of S1 Nuclease Buffer and 0.1 μl of S1 Nuclease to a final reaction volume of 30 μl with Milli-Q water. Samples lacking any enzyme were also included. The reactions were incubated at room temperature for 30 min, quenched with 2 μl of TRIS-HCl and heated at 70°C for 10 min. Each reaction was then transferred to a qPCR plate and combined with the McGill in-house qPCR Master Mix. The plate was then centrifuged in a MBI and run in the CFX96 Touch Real-Time PCR Detection System (Bio-Rad) using thermal cycling con-

ditions of 1 cycle of 25°C followed by an increase to 60°C in 0.5°C increments every 10 s.

Data analysis

SARS-CoV-2 RNA copy number approximation

A limit of detection (LOD) assay for each probe was done using a known copy number viral RNA and standard curve was generated. Subsequently, the unknown copy number SARS-CoV-2 RNA was serial diluted and amplified with each probe and Ct values were determine at each dilution factor. Using the equation of the standard curve generated from the known copy number RNA, the observed Ct values from the unknown copy number RNA amplification were used as the y-value to determine the x-value which is the approximate copy number of SARS-CoV-2 RNA.

LOD calculations

For each probe, the standard deviation (multiplied by three) of NTC amplification signals were used to determine a background threshold of 750 relative fluorescence units (RFU). Therefore, anything below 750 RFU was considered background noise. Amplification of SARS-CoV-2 RNA at ten-fold serial dilutions was detected by each probe (seven experimental replicates were done for each probe, Supplemental Fig. S1). The cycle number at which the amplification signal passes the set threshold of 750 RFU is taken as the Ct value. Ct values (cycle at which 750 RFU is reached) for each serial dilution concentrations are plotted against the approximate copies of SARS-CoV-2 RNA per reaction. The equation of the standard curve is used to find RNA copies per reaction that can be detected at Ct max of 39 cycles (Ct max determined based on the linear dynamic range of each probe). This was taken as the LOD for each probe.

Efficiency and y-intercept calculations

Probe efficiency was calculated using the equation $10^{-(1/\text{slope})} - 1$. The slope of each slope was obtained from the LOD standard curve equations generated for each probe.

The y-intercept is the cycle at which no RNA copies will be detected by the probe. Therefore, the y-intercept was calculated by determining the cycle number at which $y = 0$ using the LOD standard curve equations generated for each probe.

Results and discussion

Probe design and synthesis

A RT-qPCR probe recommended by the World Health Organization and widely used for SARS-CoV-2 testing is a 26-nucleotide long sequence targeted to the E-gene with fluorescein (FAM) at the 5′ end, and BlackBerry® Quencher (BBQ-650) at the 3′ end, **E-P0** (Supplementary Table S2) [24, 31]. However, Black Hole Quencher 1 (BHQ1) has significantly better spectral overlap with FAM than BBQ-650 [13]. Therefore, we also characterized probe **E-P1** where the BBQ-650 quencher was replaced by the BHQ1 quencher (Supplementary Table S2).

Since initial probe quenching efficiency can be improved with decreased distance between the fluorophore and the quencher [6, 23], we designed additional probes with the same sequence, but with the quencher placed at an internal position 10–11 nucleotides from the 5′ end [6, 32, 33]. However, the best way to conjugate the quencher at these two positions in a sequence independent manner was unclear. To investigate two new approaches that allow modular incorporation of various quenchers into probes in a sequence independent manner, we synthesized and evaluated probes with different linkages: **E-P2**, using a sugar-modification approach and **E-P3** via a glycerol insertion (Supplementary Table S2). In **E-P2**, the BHQ1 is conjugated to an arabino-adenosine (ara-A) branchpoint [30]. The choice of araA was based on its expected rigidity, offering a structural alternative to previously reported dT conjugates and potentially improving quenching efficiency by limiting linker flexibility [34, 35]. In contrast in **E-P3**, the BHQ1 quencher is linked to the oligonucleotide via a glycerol bulge 'X' linker that is initially introduced into the oligonucleotide containing a levulinyl (LEV) protecting group that is selectively deprotected prior to quencher introduction. This approach avoids sequence constraints imposed by nucleobase conjugates, allows compatibility with a broader range of quenchers, and facilitates modular synthesis suitable for multiplexing assays. Furthermore, the glycerol bulge 'X' linker is already a commercially available CED phosphoramidite containing the LEV protecting group or DABCYL quenching group pre-installed. [36]

Both **E-P2** and **E-P3** are capped on the 3′ end with C_3-OH group (Fig 2) to prevent the probe from acting as a primer and being extended by Taq polymerase. The probes were produced using buffered hydrazine to deprotect LEV at the branching point junction during solid-phase synthesis and purified to >80% homogeneity (Fig 2, Supplementary Table S3, and Supplementary Fig. S1). Additional probes were synthesized with matching fluorescent-quencher pairs, including an N2 gene probe for SARS-CoV-2 (**N2-P4**), Influenza A gene probe (**FluA-P5**) with Cy5 fluorophore at the 5′ end and an internal X-BHQ2, and an Influenza B gene probe (**FluB-P6**) with Cy5.5 at the 5′ end and an internal X-BBQ-650 (Supplementary Table S2).

Non-nucleoside, flexible glycerol-linkage of quencher improves probe efficiency

To determine how the structure of the linker and position of quencher influence probe performance in RT-qPCR, we made use of the RNA genome from SARS-CoV-2. By utilizing a 'one step' RT-qPCR enzyme mixture containing both reverse transcriptase and Taq polymerase, the sample RNA template was first converted into cDNA. The cDNA is then amplified by Taq polymerase through multiple cycles of cDNA denaturation, primer and probe annealing, and extension. During cDNA amplification, Taq polymerase mediates 5′→3′ hydrolysis of the fluorescent probe allowing real-time monitoring of fluorescence corresponding to the quantity of amplified SARS-CoV-2 cDNA. To compare the sensitivity and efficiency of the different probe designs, the cycle threshold (C_t) was calculated. C_t is a common qPCR parameter representing the cycle number at which the fluorescence signal surpasses the background fluorescence threshold. This value is inversely proportional to the amount of template cDNA, therefore lower C_t values are desired for better probe performance [37, 38]. Finally, the initial baseline fluorescence and the final maximal fluorescence were also measured to calculate the signal-to-noise ratio for each probe. Seven independent replicate experiments were conducted to gather statistical information (Supplementary Fig. S2).

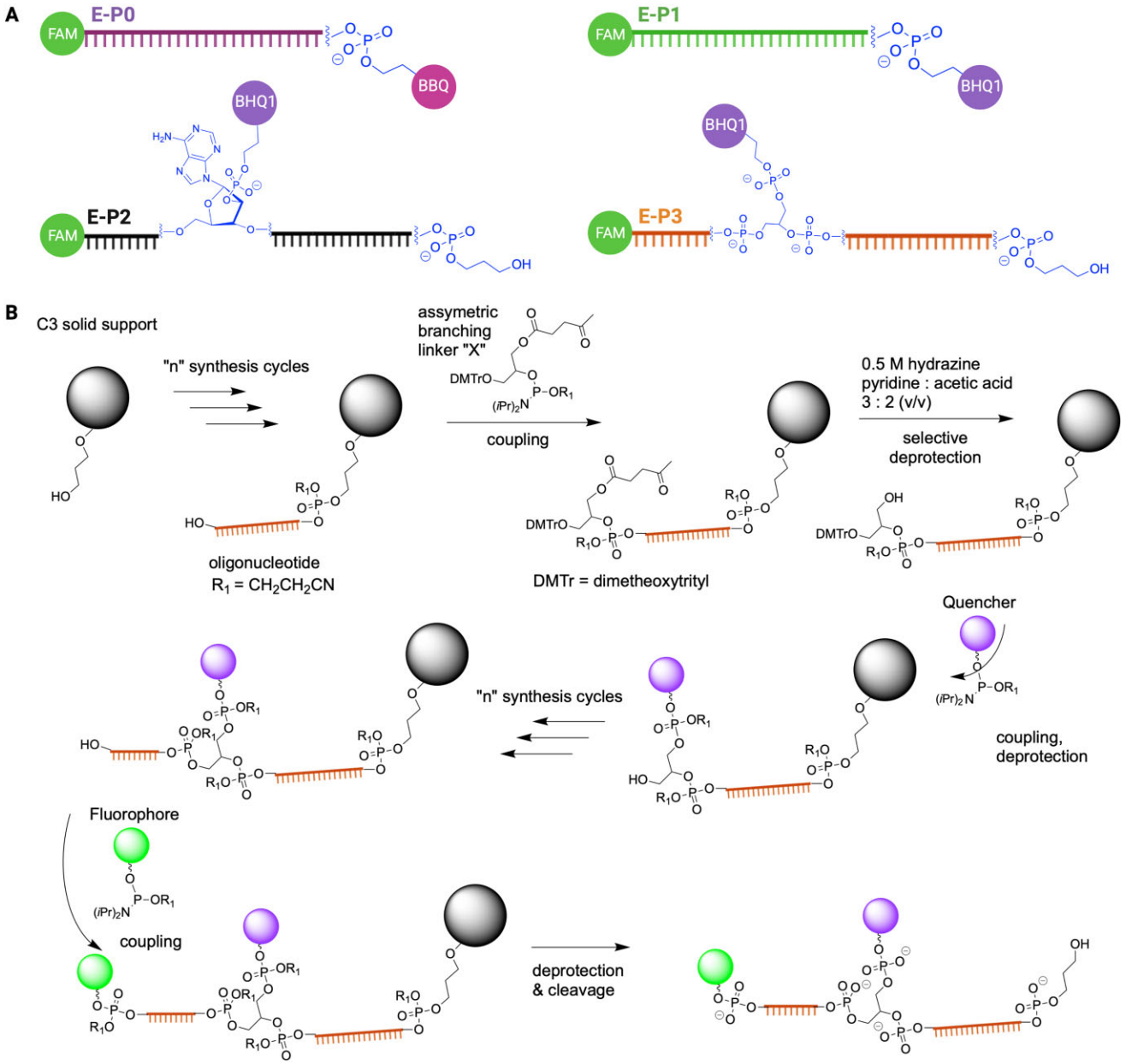

Figure 2. Design and synthesis of fluorogenic RT-qPCR probes. (**A**) Probes for the E gene of SARS-CoV-2 with FAM at the 5′ end and quencher at the 3′ end or internally linked with an OH cap at the 3′ end. (**B**) Modular, solid phase synthetic approach for producing probes containing the glycerol 'X' linker, beginning from a C3 solid support, and using buffered hydrazine to selectively deprotect LEV prior to coupling of a variable quenching group at the internal position.

Among the four probe designs for the E-gene of SARS-CoV-2, the flexible glycerol 'X' linker in **E-P3** yielded the best performance and had the lowest C_t values (Fig 3 A and B). Based on the qPCR results of a dilution series of template RNA, **E-P3** is sensitive enough to amplify RNA copy numbers as low as ~4 RNA copies per reaction (Fig 3C and F), with signals in the same range as the maximum fluorescent signal of **E-P1** and **E-P0** probes. In comparison, the LOD for probe **E-P0** was ~11 copies per reaction and for probe **E-P1** was ~17 copies per reaction (Fig 3C–E). A comparison of probe efficiencies revealed that **E-P3** performed the best, with an efficiency >90% (Fig 3G) and the lowest y-intercept, indicating the cycle at which a $\log_{10}$ RNA copy number, equivalent to one RNA copy, can be detected (Fig 3H). When comparing the initial and final uncorrected fluorescence (RFU), the **E-P0** probe starts with a high initial background fluorescence, resulting in a low signal-to-noise ratio in the final fluorescence, hence, reducing the capacity to detect small changes in fluorescence signals (Fig 3I). The **E-P1** probe starts at a lower background fluorescence signal; however, the maximal fluorescence of the **E-P1** probe is also low, indicating poor cleavage efficiency of the probe. As such, the signal-to-noise ratio is also small due to the small difference between the initial and final uncorrected RFUs (Fig 3I). Interestingly, **E-P3** showed the best signal-to-noise ratio due to the very low initial fluorescence and significantly higher maximal fluorescence (Fig 3I). When the probes were tested with a commercially available one-step RT-qPCR master mix, similar results were obtained (Supplementary Fig. S3).

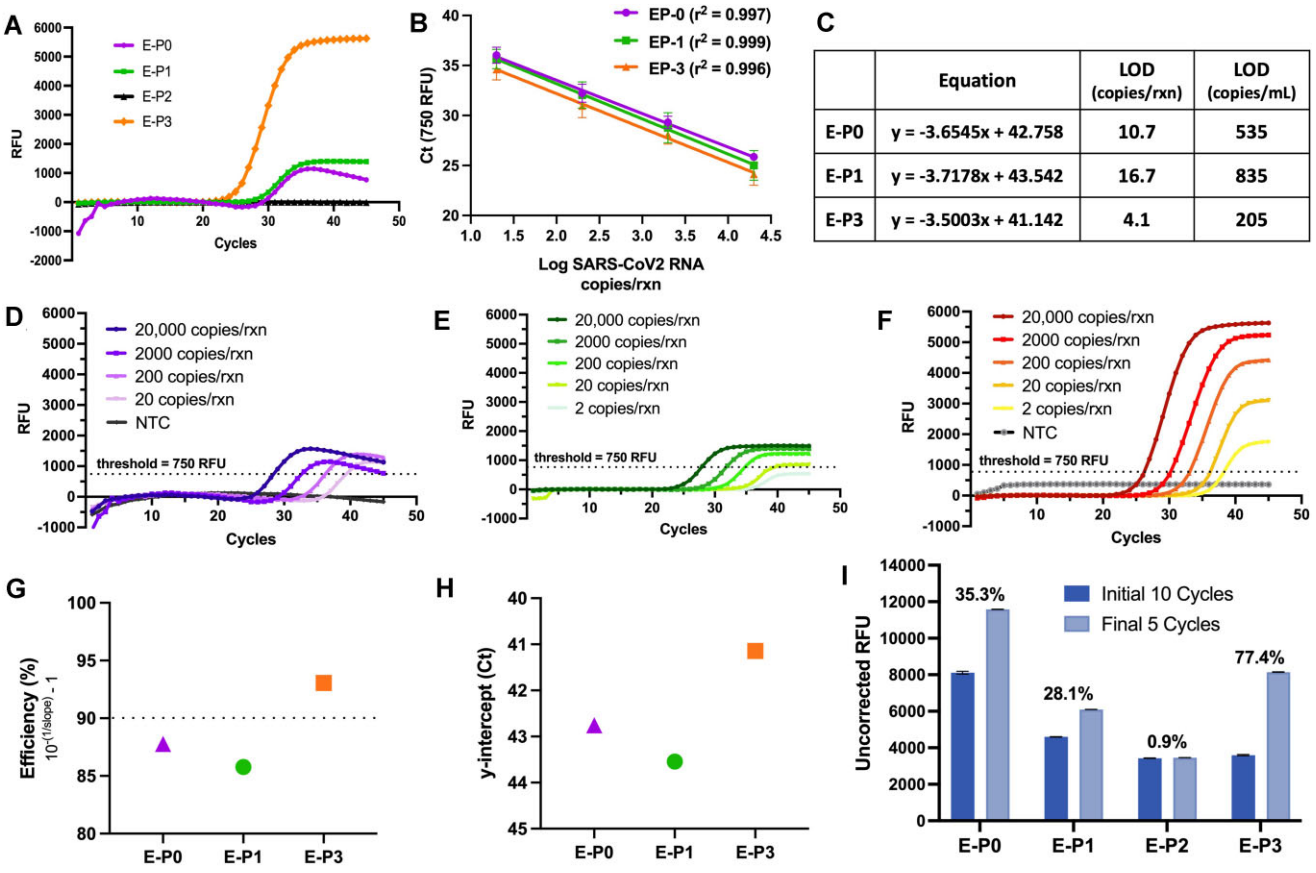

	Equation	LOD (copies/rxn)	LOD (copies/mL)
E-P0	y = -3.6545x + 42.758	10.7	535
E-P1	y = -3.7178x + 43.542	16.7	835
E-P3	y = -3.5003x + 41.142	4.1	205

Figure 3. X-linked quencher improves probe efficiency. (**A**) qPCR plots obtained in the presence of 20 000 SARS-CoV-2 RNA copies/reaction for each E-gene probe; annealing temperature of 60°C was used. (**B**) C_t versus $\log_{10}$ (RNA copies) for seven experimental replicates. (**C**) Calculated LOD from seven experimental replicates. (**D**) **E-P0**; (**E**) **E-P1**; and (**F**) **E-P3** at different copy numbers of RNA. (**G**) Comparison of probe efficiencies [slope of equations in panel (C)]. (**H**) y-intercept (Ct) showing the cycle at which $\log_{10}$ (RNA copies), which is equivalent to one RNA copy, is detected. (**I**) The average and standard deviation of the initial and final uncorrected fluorescence from each probe during RT-qPCR and 20 000 SARS-CoV-2 copies/reaction (samples run in triplicate).

E-P2 probe hybridizes to complementary sequences but is not cleaved by Taq polymerase

The differences in fluorescence changes observed between the linker chemistries used in the internal placement of quenchers in the **E-P2** and **E-P3** probes were unexpected. To investigate the underlying mechanism for this altered performance, we analyzed cDNA amplification and probe hydrolysis during qPCR, as well as the probe hybridization under varying temperature conditions. We first analyzed products of the RT-qPCR reactions on a denaturing polyacrylamide gel electrophoresis (PAGE). All reactions, including those using the **E-P2** probe showed a clear product band of correct size for the DNA amplicon of the desired PCR reaction (Fig 4A, yellow arrow). This confirms that PCR amplification of the viral RNA occurred even though the **E-P2** probe did not provide any increased fluorescence during the cycles.

We next examined whether the conjugation strategies altered probe binding affinity to the DNA amplicon of the PCR reaction using thermal denaturation analysis of each probe in the presence of an excess of DNA that is complementary to the probe. The melting analyses were performed by tracking fluorescence changes in the presence of the qPCR Master Mix and data corrected by subtracting background changes of the mix only. First derivative analyses of the corrected data were used to determine melting temperatures (T_m). The results suggest that all four probes bind to cDNA to form stable duplexes with T_m values ranging from 57.3–67.4°C (Fig 4C–F). The **E-P2** probe duplex exhibited the lowest T_m value (57.3°C) near the 60°C annealing/extension temperature used in standard RT-qPCR reactions. The reduced T_m of **E-P2** likely results from the arabinose linker modification, where the 2′-OH group introduces steric clashes with base protons (H6/H8), disrupting base stacking interactions that are critical for duplex stability [34, 35, 39]. Additionally, the O4′-endo sugar pucker preference of arabinose may further destabilize the structure [34, 35, 39]. To verify that the lack of amplification signal with the **E-P2** probe was not a result of using too high of an annealing temperature (e.g. higher than its measured T_m), we conducted the same experiment using a lower annealing temperature of 55°C. However, even at this lower temperature, no amplification signal was observed for **E-P2** (Supplementary Fig. S4). Moreover, the lower annealing temperature negatively impacted the signal of the other probes, resulting in higher Ct values and a significant decrease in the RFU signal for the best-performing probe, **E-P3**.

Some fluorescence melting behavior, however, was also exhibited by all four probes in the absence of cDNA (Supplementary Fig. S5). To ensure that the melting curves represented hybridization to the complement, we further evaluated probe-amplicon binding via fluorescence polarization,

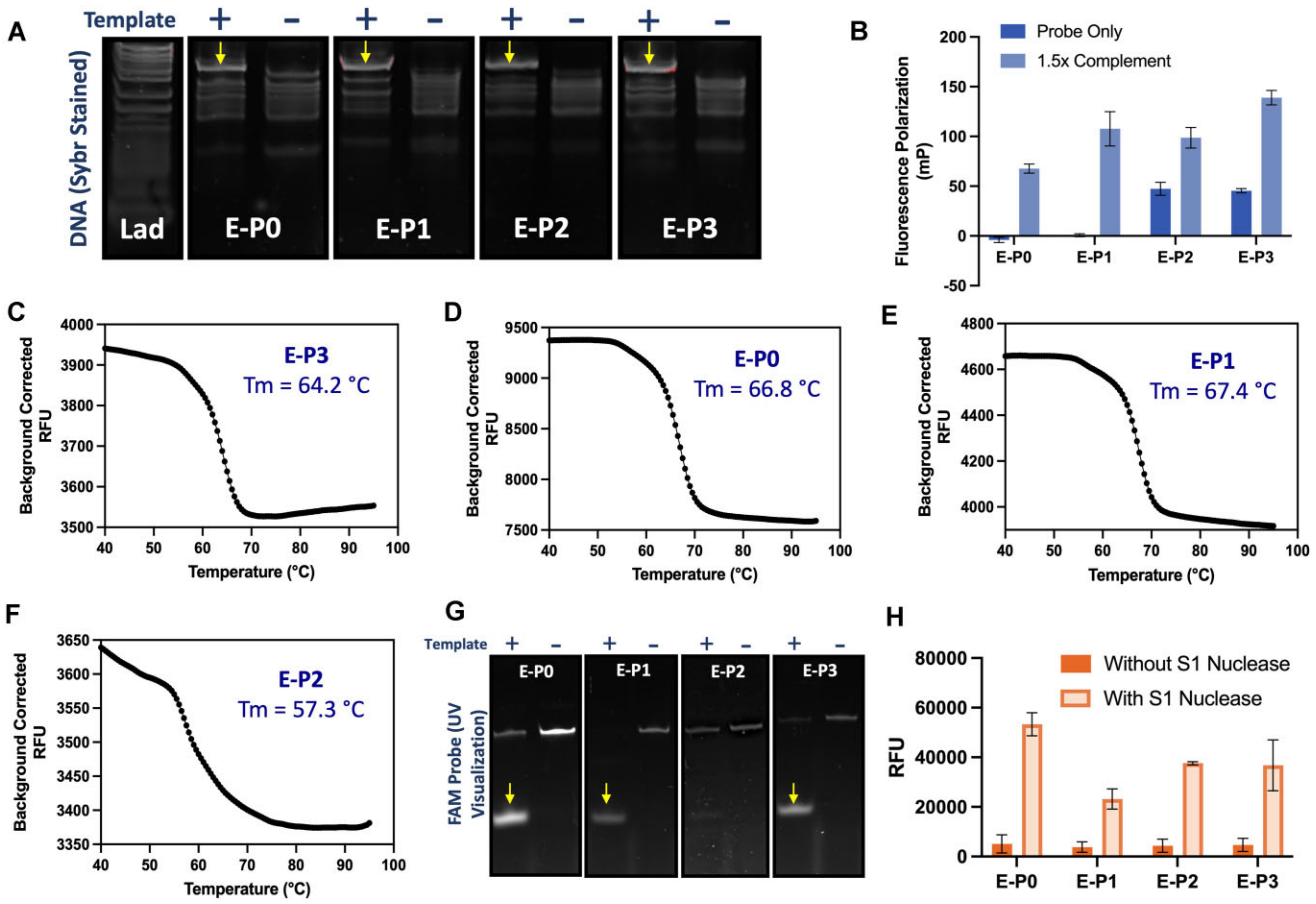

Figure 4. E-P2 hybridizes to complementary sequences but is not cleaved by Taq polymerase. (**A**) Ten percent denaturing PAGE stained with SYBR Safe analyzing the qPCR reaction products generated in the absence and presence of SARS-CoV-2 RNA (2000 copies/reaction). Small arrows indicate the desired SARS-CoV-2 amplification product. (**B**) Fluorescence polarization analysis of probes in the presence or absence of 1.5 eq. of cDNA oligonucleotide measured at 60 °C. The means and standard deviations of three technical replicates are given. (**C–F**) Thermal denaturation and T_m (calculated by first-derivative analysis) of probe with 1.5× complementary sequence. (**G**) Visualizing fluorescence from each probe in a 10% denaturing PAGE gel. Small arrows indicate cleaved probe. (**H**) Fluorescence intensities of probes following incubation with or without S1 nuclease. Data are the mean and standard deviation of three technical replicates.

where the degree of polarization is inversely related to the molecular dynamics of the fluorescent probe and fluorescence lifetime of the fluorophore [40]. The end-labeled probes **E-P0** and **E-P1** probes exhibited the lowest fluorescence polarization values in the absence of the cDNA strand, while **E-P2** and **E-P3** exhibited comparatively higher polarization values (Fig 4B). Upon addition of 1.5 eq. of cDNA, all probes exhibited a 50–100 mP increase in polarization, consistent with amplicon binding and the formation of duplex structures for all four probes [41].

To determine whether the probes were hydrolytically cleaved by Taq during RT-qPCR, the reaction products following thermocycling in the presence and absence of SARS-CoV-2 RNA were analyzed via PAGE. In all reactions lacking the template, a high molecular weight band is observed, representing the full-length, uncleaved probe (Fig 4G). Reactions conducted in the presence of target RNA contained a brighter, probe cleavage product with higher electrophoretic mobility for probes **E-P0**, **E-P1**, and **E-P3**, but not **E-P2** (Fig 4G, yellow arrows). Together, these results suggest that while the probe binds to the template, and that amplification can still proceed, Taq is unable to cleave **E-P2** and thus does not generate a quantitative fluorescence readout of amplification. To rule out the unlikely possibility that differences in linker chemistry can somehow cause fluorescein bleaching, the probes were extensively digested with S1 nuclease and fluorescence changes measured. All four probes including **E-P2** displayed high fluorescence in the presence of S1 nuclease indicating probe cleavage and thus separation of the fluorophore from the quencher (Fig 4H). As such, **E-P2** is capable of being cleaved, and it can hybridize to the DNA amplicon; however, upon primer extension, the probe is displaced from the template rather than being cleaved.

E-P3 has robust efficiency in multiplexed RT-qPCR

Having established the utility of a new, glycerol 'X' linker for sensitive qPCR-based detection of SARS-CoV-2 by targeting the E gene, we next wanted to explore its utility in probes to other viral RNA sequences in multiplexed RT-qPCR. For the **N2-P4** probe targeting SARS-CoV-2 N-gene we used the HEX fluorophore and a BHQ1 quencher. To detect Influenza A, the probe **FluA-P5** was tagged with the Cy5 fluorophore and BHQ2 quencher. Finally, to detect Influenza B, we used the **FluB-P6** with a Cy5.5 fluorophore and BBQ quencher. For all the probes, the flexible 'X' linker was used for internal placement of the corresponding quenchers. Reaction mixtures were prepared containing the qPCR Master Mix and all eight

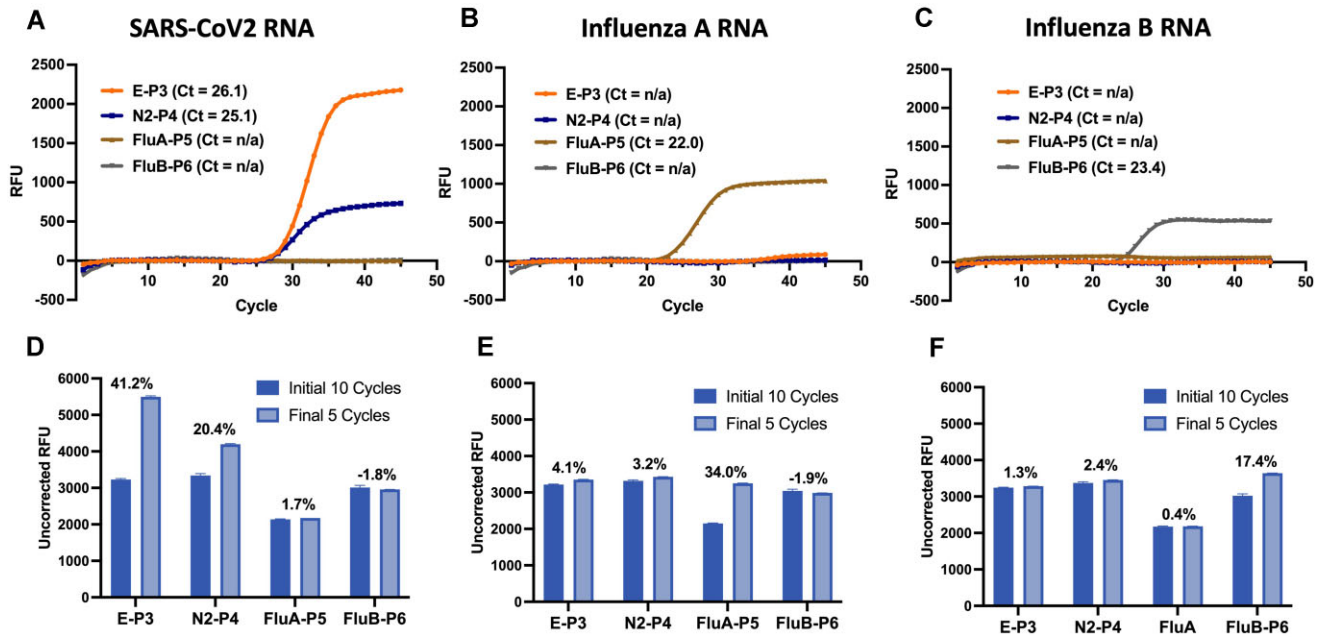

Figure 5. E-P3 has robust efficiency in multiplexed RT-qPCR. (**A–C**) Tetraplexing RT-qPCR results of reaction mixtures containing equimolar mixtures of **E-P3**, **N2-P4**, **FluA-P5**, and **FluB-P6** probes and RNA added from SARS-CoV-2, Influenza A, or Influenza B. (**D–F**) The average initial and final uncorrected fluorescence of each probe in tetraplexing reactions containing; (**D**) 20 000 SARS-CoV-2 RNA copies/reaction; (**E**) 50 000 Influenza A RNA copies/reaction; (**F**) 50 000 Influenza B RNA copies/reaction. Data are the mean and standard deviation of three technical replicates. See Supplementary Fig. S6 for results obtained using fewer RNA copy numbers.

primers and four probes for the four different target RNAs. Using this reaction mixture, when SARS-CoV-2 RNA template was added and measured via qPCR, only the fluorescein and HEX signals from **E-P3** and **N2-P4** probes respectively were detected (Fig 5A and D) – no Cy5 and Cy5.5 fluorescence was observed even after 45 cycles of amplification. Similarly, when either the Influenza A target or the Influenza B RNA were added to the reaction, only Cy5 fluorescence from **FluA-P5** or Cy5.5 fluorescence from **FluB-P6** probe, respectively, were detected due to the selective amplification of the respective templates (Fig 5B, C, E, and F). In the tetraplex format, as little as 20 copies of SARS-Co-V genome could be readily distinguished from 50 copies of Flu-A or 50 copies of Flu-B genomes in a single reaction (Supplementary Fig. S6). Indeed, the utility of the glycerol-based linker extends beyond single-target assays. This multiplex capability, combined with the probe's superior performance, underscores its potential for high-throughput clinical diagnostics.

In conclusion, our study highlights the critical role of probe design for enhancing the efficiency and sensitivity of RT-qPCR assays. By systematically evaluating the impact of quencher placement and linker chemistry using a SARS-CoV-2 E-gene probe as a model system, we demonstrated the advantages of a glycerol-based 'X' linker over traditional 3′-end quenchers and internal arabinoside-based linkers. This non-nucleoside bulge design not only enhances quenching efficiency but also avoids sequence constraints imposed by nucleobase conjugates, thereby enabling a broader range of target applications (Supplementary Table S4).

The glycerol-based 'X' linker significantly enhances the signal-to-noise ratio and overall sensitivity compared to traditional end-labeled probes. This design not only allows for the detection of very low RNA concentrations, but also improves the accuracy of diagnosis, especially in distinguishing between similar viral infections. Additionally, the flexibility in the probe backbone, facilitated by the 'X' linker, further contributes to the probe's superior performance by optimizing the interaction with Taq polymerase during the PCR process. These findings underscore the importance of strategic probe design, particularly the internal linkage of quenchers, in developing more effective and reliable molecular diagnostics. The glycerol-based 'X' linker offers a practical and scalable solution for developing sensitive, efficient, and robust diagnostic assays. This approach could be especially valuable in pandemic situations, where rapid, accurate, and sensitive testing is paramount. Future studies could explore its adaptation to other probe designs and diagnostic platforms, further broadening its impact in clinical and research settings.

Acknowledgements

Authors thank T.M. Schmeing, G. Pelletier, L.L. Shen, J.-F. Trempe, and A.N. Bayne for the RT-qPCR master mix used in most experiments [29] and Dr John Randolph for helpful discussions. We would like to thank Micaela Belleperche for assisting with polarization experiments. We thank the McGill Chemistry Characterization Facility for providing instrumentation and resources for LC-MS-based characterization and analysis. We thank members of the McKeague, Damha, and Luedtke labs for useful discussions. Graphical abstract was created in BioRender. Maru, B. (2025) https://BioRender.com/c66m289.

Author contributions: M.D., N.W.L., and M.M conceptualized the project. A.K., R.E.K., and K.B. synthesized and purified the probes. B.M. and A.E. carried out the experiments. A.S.W. performed the mass spectrometry characterization. B.M., M.M., N.W.L., and A.E. analyzed the data while

M.M., N.W.L., and B.M. wrote the paper and all authors reviewed the paper.

Supplementary data

Supplementary data is available at NAR online.

Conflict of interest

None declared.

Funding

This work was supported by the Faculty of Science at McGill University, by a Fonds de Recherche du Québec (FRQ-S, Health Sector) Research Centres Grant #288558, through the Natural Sciences and Engineering Research Council of Canada (Discovery Grants 2019-04949 to M.M., 2020-05048 to N.L., and 2016-05126 to M.D.), the Canada Foundation for Innovation (JELFs to M.M. and N.W.L), and the Canada First Research Excellence Fund, D2R (Foundational Project Grant to N.W.L., M.M., and M.D.). B.M. is supported by awards from the Canadian Institutes of Health Research and FRQ-S; B.M. and A.E. were supported through awards from NSERC CREATE PROMOTE.

Data availability

The data underlying this article are available in the article and in its online supplementary material.

References

1. Mackay IM, Arden KE, Nitsche A. Real-time PCR in virology. *Nucleic Acids Res* 2002;**30**:1292–305. https://doi.org/10.1093/nar/30.6.1292
2. Taylor SC, Nadeau K, Abbasi M *et al.* The ultimate qPCR experiment: producing publication quality, reproducible data the first time. *Trends Biotechnol* 2019;**37**:761–74. https://doi.org/10.1016/j.tibtech.2018.12.002
3. Gudnason H, Dufva M, Bang DD *et al.* Comparison of multiple DNA dyes for real-time PCR: effects of dye concentration and sequence composition on DNA amplification and melting temperature. *Nucleic Acids Res* 2007;**35**:e127. https://doi.org/10.1093/nar/gkm671
4. Higuchi R, Dollinger G, Walsh PS *et al.* Simultaneous amplification and detection of specific DNA sequences. *Nat Biotechnol* 1992;**10**:413–7. https://doi.org/10.1038/nbt0492-413
5. Cao H, Shockey JM. Comparison of TaqMan and SYBR Green qPCR methods for quantitative gene expression in tung tree tissues. *J Agric Food Chem* 2012;**60**:12296–303. https://doi.org/10.1021/jf304690e
6. Proudnikov D, Yuferov V, Zhou Y *et al.* Optimizing primer–probe design for fluorescent PCR. *J Neurosci Methods* 2003;**123**:31–45. https://doi.org/10.1016/S0165-0270(02)00325-4
7. Bustin S. Quantification of mRNA using real-time reverse transcription PCR (RT-PCR): trends and problems. *J Mol Endocrinol* 2002;**29**:23–39. https://doi.org/10.1677/jme.0.0290023
8. Holland PM, Abramson RD, Watson R *et al.* Detection of specific polymerase chain reaction product by utilizing the 5′–3′ exonuclease activity of Thermus aquaticus DNA polymerase. *Proc Natl Acad Sci USA* 1991;**88**:7276–80. https://doi.org/10.1073/pnas.88.16.7276
9. Lee LG, Connell CR, Bloch W. Allelic discrimination by nick-translation PCR with fluorogenic probes. *Nucl Acids Res* 1993;**21**:3761–6. https://doi.org/10.1093/nar/21.16.3761
10. Heid CA, Stevens J, Livak KJ *et al.* Real time quantitative PCR. *Genome Res* 1996;**6**:986–94. https://doi.org/10.1101/gr.6.10.986
11. Livak KJ, Flood SJ, Marmaro J *et al.* Oligonucleotides with fluorescent dyes at opposite ends provide a quenched probe system useful for detecting PCR product and nucleic acid hybridization. *Genome Res* 1995;**4**:357–62. https://doi.org/10.1101/gr.4.6.357
12. Hawkins SFC, Guest PC. Multiplex analyses using real-time quantitative PCR. *Methods Mol Biol* 2017;**1546**:125–33. https://doi.org/10.1007/978-1-4939-6730-8_8
13. Marras SA. Interactive fluorophore and quencher pairs for labeling fluorescent nucleic acid hybridization probes. *Mol Biotechnol* 2008;**38**:247–55. https://doi.org/10.1007/s12033-007-9012-9
14. Hirotsu Y, Maejima M, Shibusawa M *et al.* Pooling RT-qPCR testing for SARS-CoV-2 in 1000 individuals of healthy and infection-suspected patients. *Sci Rep* 2020;**10**:18899. https://doi.org/10.1038/s41598-020-76043-z
15. Kramer MF. Stem-loop RT-qPCR for miRNAs. *Curr Protoc Mol Biol* 2011;**95**:Unit 15.10. https://doi.org/10.1002/0471142727.mb1510s95
16. Han YJ, Liu LY, Liu QQ *et al.* Optimization and performance evaluation of double-stranded probe in real-time PCR. *Anal Biochem* 2022;**650**:114711. https://doi.org/10.1016/j.ab.2022.114711
17. Wang C, Yang CJ. In: Yang CJ, Tan W (eds.), *Molecular Beacons*. Springer Berlin Heidelberg, Berlin, Heidelberg, 2013, 45–59.
18. Navarro E, Serrano-Heras G, Castaño MJ *et al.* Real-time PCR detection chemistry. *Clin Chim Acta* 2015;**439**:231–50. https://doi.org/10.1016/j.cca.2014.10.017
19. Buh Gašparič M, Tengs T, La Paz JL *et al.* Comparison of nine different real-time PCR chemistries for qualitative and quantitative applications in GMO detection. *Anal Bioanal Chem* 2010;**396**:2023–9. https://doi.org/10.1007/s00216-009-3418-0
20. Thelwell N, Millington S, Solinas A *et al.* Mode of action and application of Scorpion primers to mutation detection. *Nucleic Acids Res* 2000;**28**:3752–61. https://doi.org/10.1093/nar/28.19.3752
21. Ballantyne KN, van Oorschot RA, Mitchell RJ. Locked nucleic acids in PCR primers increase sensitivity and performance. *Genomics* 2008;**91**:301–5. https://doi.org/10.1016/j.ygeno.2007.10.016
22. Wilson PM, Labonte MJ, Russell J *et al.* A novel fluorescence-based assay for the rapid detection and quantification of cellular deoxyribonucleoside triphosphates. *Nucleic Acids Res* 2011;**39**:e112. https://doi.org/10.1093/nar/gkr350
23. Demuth J, Kantor M, Kucera R *et al.* Comparison of quenching efficiencies in long triple-labeled and double-labeled TaqMan oligodeoxynucleotide probes. *Bioconjug Chem* 2022;**33**:788–94. https://doi.org/10.1021/acs.bioconjchem.2c00023
24. Corman VM, Landt O, Kaiser M *et al.* Detection of 2019 novel coronavirus (2019-nCoV) by real-time RT-PCR. *Eurosurveillance* 2020;**25**:2000045. https://doi.org/10.2807/1560-7917.ES.2020.25.3.2000045
25. Ryazantsev DY, Tsybulsky DA, Prokhorenko IA *et al.* Two-dye and one- or two-quencher DNA probes for real-time PCR assay: synthesis and comparison with a TaqMan™ probe. *Anal Bioanal Chem* 2012;**404**:59–68. https://doi.org/10.1007/s00216-012-6114-4
26. Chu DKW, Pan Y, Cheng SMS *et al.* Molecular diagnosis of a novel coronavirus (2019-nCoV) causing an outbreak of pneumonia. *Clin Chem* 2020;**66**:549–55. https://doi.org/10.1093/clinchem/hvaa029
27. Rai P, Kumar BK, Deekshit VK *et al.* Detection technologies and recent developments in the diagnosis of COVID-19 infection. *Appl Microbiol Biotechnol* 2021;**105**:441–55. https://doi.org/10.1007/s00253-020-11061-5

28. Dutta D, Naiyer S, Mansuri S *et al.* COVID-19 diagnosis: a comprehensive review of the RT-qPCR method for detection of SARS-CoV-2. *Diagnostics (Basel)* 2022;**12**:1503. https://doi.org/10.3390/diagnostics12061503
29. Schmeing TM, Pelletier G, Shen LL *et al.* WO/2022/201104 - Compositions, methods andkits comprising polyinosinic acid (poly(i)) for Polymerase Chain Reaction (PCR).
30. Katolik A, Johnsson R, Montemayor E *et al.* Regiospecific solid-phase synthesis of branched oligoribonucleotides that mimic intronic lariat RNA intermediates. *J Org Chem* 2014;**79**:963–75. https://doi.org/10.1021/jo4024182
31. WHO. *Novel Coronavirus (2019-nCoV) Technical Guidance: Laboratory Testing for 2019-nCoV in Humans*. Geneva, Switzerland: World Health Organization, 2020.
32. Ju J, Glazer AN, Mathies RA. Cassette labeling for facile construction of energy transfer fluorescent primers. *Nucleic Acids Res* 1996;**24**:1144–8. https://doi.org/10.1093/nar/24.6.1144
33. Ju J, Ruan C, Fuller CW *et al.* Fluorescence energy transfer dye-labeled primers for DNA sequencing and analysis. *Proc Natl Acad Sci USA* 1995;**92**:4347–51. https://doi.org/10.1073/pnas.92.10.4347
34. Denisov AY, Noronha AM, Wilds CJ *et al.* Solution structure of an arabinonucleic acid (ANA)/RNA duplex in a chimeric hairpin: comparison with 2′-fluoro-ANA/RNA and DNA/RNA hybrids. *Nucleic Acids Res* 2001;**29**:4284–93. https://doi.org/10.1093/nar/29.21.4284
35. Watts JK, Damha MJ. 2′ F-Arabinonucleic acids (2′ F-ANA)—history, properties, and new frontiers. *Can J Chem* 2008;**86**:641–56. https://doi.org/10.1139/v08-049
36. Katolik A, Clark NE, Tago N *et al.* Fluorescent branched RNAs for high-throughput analysis of Dbr1 enzyme kinetics and inhibition. *ACS Chem Biol* 2017;**12**:622–7. https://doi.org/10.1021/acschembio.6b00971
37. Livak KJ, Schmittgen TD. Analysis of relative gene expression data using real-time quantitative PCR and the 2−ΔΔCT method. *Methods* 2001;**25**:402–8. https://doi.org/10.1006/meth.2001.1262
38. Rao X, Huang X, Zhou Z *et al.* An improvement of the 2ˆ (-delta delta CT) method for quantitative real-time polymerase chain reaction data analysis. *Biostat Bioinforma Biomath* 2013;**3**:71–85.
39. Martín-Pintado N, Yahyaee-Anzahaee M, Campos-Olivas R *et al.* The solution structure of double helical arabino nucleic acids (ANA and 2′F-ANA): effect of arabinoses in duplex-hairpin interconversion. *Nucleic Acids Res* 2012;**40**:9329–39. https://doi.org/10.1093/nar/gks672
40. Checovich WJ, Bolger RE, Burke T. Fluorescence polarization—a new tool for cell and molecular biology. *Nature* 1995;**375**:254–6. https://doi.org/10.1038/375254a0
41. Hudson RHE, Ganeshan K, Damha MJ. *Carbohydrate Modifications in Antisense Research*. American Chemical Society, 1994, **580**, 133–52.

Received: October 15, 2024. **Revised:** January 25, 2025. **Editorial Decision:** February 10, 2025. **Accepted:** February 16, 2025